Structural analysis of 14-3-3-ζ-derived phosphopeptides using electron capture dissociation mass spectrometry, traveling wave ion mobility spectrometry, and molecular modeling

Simmonds, Anna; Lopez-Clavijo, Andrea; Winn, Peter; Russell, David; Styles, Iain; Cooper, Helen

DOI:
10.1021/acs.jpcb.9b08506

Document Version
Publisher's PDF, also known as Version of record

Citation for published version (Harvard):
Simmonds, A, Lopez-Clavijo, A, Winn, P, Russell, D, Styles, I & Cooper, H 2020, 'Structural analysis of 14-3-3-ζ-derived phosphopeptides using electron capture dissociation mass spectrometry, traveling wave ion mobility spectrometry, and molecular modeling', *Journal of Physical Chemistry B*, vol. 124, no. 3, pp. 461-469. https://doi.org/10.1021/acs.jpcb.9b08506

THE JOURNAL OF PHYSICAL CHEMISTRY B

Article

Cite This: J. Phys. Chem. B 2020, 124, 461−469

pubs.acs.org/JPCB

Structural Analysis of 14-3-3-ζ-Derived Phosphopeptides Using Electron Capture Dissociation Mass Spectrometry, Traveling Wave Ion Mobility Spectrometry, and Molecular Modeling

Anna L. Simmonds,[†,‡,#] Andrea F. Lopez-Clavijo,[†,#,▽] Peter J. Winn,[†] David H. Russell,[∥] Iain B. Styles,[§,⊥] and Helen J. Cooper*[,†]

[†]School of Biosciences, [‡]Physical Sciences for Health CDT, and [§]School of Computer Science, University of Birmingham, Birmingham B15 2TT, U.K

[∥]Texas A&M University, College Station, Texas 77843, United States

[⊥]Centre of Membrane Proteins and Receptors (COMPARE), Universities of Birmingham and Nottingham, Midlands, U.K

Supporting Information

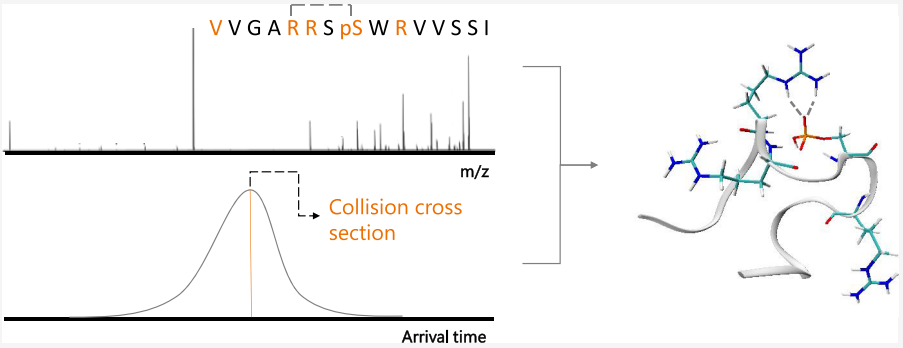

ABSTRACT: Previously, we have demonstrated the effect of salt bridges on the electron capture dissociation mass spectrometry behavior of synthetic model phosphopeptides and applied an ion mobility spectrometry/molecular modeling approach to rationalize the findings in terms of peptide ion structure. Here, we develop and apply the approach to a biologically derived phosphopeptide. Specifically, we have investigated variants of a 15-mer phosphopeptide VVGARRSsWRVVSSI (s denotes phosphorylated Ser) derived from Akt1 substrate 14-3-3-ζ, which contains the phosphorylation motif RRSsWR. Variants were generated by successive arginine-to-leucine substitutions within the phosphorylation motif. ECD fragmentation patterns for the eight phosphopeptide variants show greater sequence coverage with successive R → L substitutions. Peptides with two or more basic residues had regions with no sequence coverage, while full sequence coverage was observed for peptides with one or no basic residues. For three of the peptide variants, low-abundance fragments were observed between the phosphoserine and a basic residue, possibly due to the presence of multiple conformers with and without noncovalent interactions between these residues. For the five variants whose dissociation behavior suggested the presence of intramolecular noncovalent interactions, we employed ion mobility spectrometry and molecular modeling to probe the nature of these interactions. Our workflow allowed us to propose candidate structures whose noncovalent interactions were consistent with the ECD data for all of the peptides modeled. Additionally, the AMBER parameter sets created for and validated by this work are presented and made available online (http://www.biosciences-labs.bham.ac.uk/cooper/datasets.php).

INTRODUCTION

Electron capture dissociation (ECD)[1] is a fragmentation technique typically employed in Fourier transform ion cyclotron resonance (FT-ICR) mass spectrometers and, more recently, in other mass spectrometers by the addition of a linear ECD cell.[2,3] ECD makes use of low-energy electrons to irradiate multiply charged analyte ions and induce fragmentation. In proteins and peptides, cleavages at the N−Cα bond are preferred, while labile post-translational modifications (PTMs), such as phosphorylation, are retained on the backbone fragment, enabling localization of modification sites in proteins and peptides.[4−8] A particular feature of ECD is the preservation of noncovalent interactions.[9,10] (Evidence for the presence of noncovalent interactions in the gas phase has been provided by blackbody infrared dissociation studies of bradykinin[11] and multiple studies showing the preservation of noncovalently bound protein−ligand complexes.)[12−15] This feature of ECD has enabled its use as a probe of protein structure by inferring that regions of poor fragment coverage by ECD have more noncovalent inter-

Received: September 6, 2019
Revised: December 19, 2019
Published: December 20, 2019

DOI: 10.1021/acs.jpcb.9b08506
J. Phys. Chem. B 2020, 124, 461−469

Table 1. Model Peptide Sequences[a]

peptide sequence	abbreviated name	monoisotopic mass (Da)	$[M + 2H]^{2+}$ (m/z)	$^{TW}CCS_{N2\rightarrow He}$ (Å^2)
VVGA**RR**S**s**W**R**VVSSI	Pep-01	1737.27158	869.64307	354.82 ± 0.74
VVGA**R**LS**s**W**R**VVSSI	Pep-02	1694.25453	848.13455	346.17 ± 1.05
VVGA**RR**S**s**WLVVSSI	Pep-03	1694.25453	848.13455	329.55 ± 0.65
VVGAL**RS**s**W**RVVSSI	Pep-04	1694.25453	848.13455	333.42 ± 1.10
VVGA**R**LS**s**WLVVSSI	Pep-05	1609.19053	805.60255	332.47 ± 0.49
VVGAL**RS**s**W**LVVSSI	Pep-06	1609.19053	805.60255	331.42 ± 1.91
VVGALLS**s**W**R**VVSSI	Pep-07	1609.19053	805.60255	336.19 ± 1.39
VVGALLS**s**WLVVSSI	Pep-08	1608.22043	805.11750	329.73 ± 0.65

[a]Arginine and phosphoserine residues are shown in bold.

actions and therefore more rigid structures. ECD studies of the IR-induced unfolding of ubiquitin ions showed the differences between solution- and gas-phase unfolding pathways,[16] with later work focusing on the unfolding of ubiquitin ions via desolvation.[17] In a study of the protein KIX, the presence of noncovalent interactions was shown to increase the longevity of the native solution-phase structure in the gas phase.[18] A study combining ECD and ion mobility spectrometry (IMS) data allowed the extent and location of collision-induced unfolding in human hemoglobin to be discerned,[19] while similar techniques were used to study the unfolding landscape of both the wild type and mutants of the protein Ltn.[20] Similarly, electron transfer dissociation (ETD), an electron-based dissociation method similar to ECD, has been used in conjunction with IMS to study the unfolding of several proteins.[21] ETD has also been used to predict intramolecular salt-bridge locations in several proteins by observing regions of the peptide sequence without fragment coverage. These proposed salt-bridge locations were then compared to all possible salt bridges and were found to closely resemble the salt bridges of the native protein structures.[22,23] It has been shown that both ECD and ETD can be used to determine the site of intermolecular interactions between acidic and basic peptides.[12]

We have shown previously that reduced ECD sequence coverage is observed in a suite of synthetic phosphopeptides based on the sequence APLSFRGSLPKSYVK, particularly in peptides containing two or more basic residues.[24] We concluded that this observation was the result of salt-bridge interactions between the phosphate and the basic residues. This conclusion was in agreement with prior ion mobility spectrometry experiments, which revealed that phosphopeptides have lower CCS than would be predicted for a random coil.[25−27] This compaction has been attributed to noncovalent interactions between the phosphate group and positively charged residues in the peptide sequence.[25] In more recent work, we showed that the presence of phosphorylated serine and basic amino acids alone (in peptides that otherwise only contained alanine and proline residues) was insufficient to inhibit ECD fragmentation and that the conformation of the peptide (and therefore the relative positions of the interacting residues) was important in determining ECD behavior.[28]

Further work on the APLSFRGSLPKSYVK phosphopeptides used an ion mobility spectrometry/molecular modeling (MM) approach to assess whether model structures could rationalize the observed ECD behavior.[29] The combined application of IMS and MM is a well-established approach for the investigation of gas-phase ion structure. That is, collision cross sections (CCS) are derived from IMS experiments and compared with those calculated for molecular models, enabling the viability of candidate structures to be assessed.[30] Traveling wave ion mobility spectrometry (TWIMS) is one such IMS platform[31] through which CCS can be calculated from an ion's arrival time by means of a calibration to reference standards.[32] TWIMS and MM have been successfully combined for structural studies of various molecular classes including drugs,[33] nucleic acids,[34] peptides,[35] and proteins and their complexes.[36]

Here, we have combined ECD, TWIMS, and MM for the study of the RRSsWR phosphorylation motif, from the 15-mer phosphopeptide VVGARRSsWRVVSSI (s denotes phosphorylated Ser) found in the Akt1 substrate 14-3-3-ζ. The S58 residue of 14-3-3-ζ has been shown to be phosphorylated in vivo by PKB/Akt[37] and SDK.[38] Successive arginine-to-leucine substitutions allowed us to examine the effect of multiple positive-charge carriers on ECD behavior. Further, we found that our approach allowed us to propose candidate structures consistent with the ECD and IMS data for all peptides investigated and interrogate their possible protonation patterns and conformers.

MATERIALS AND METHODS

Materials. Model peptides were synthesized by GenicBio (Shanghai, China) and used without further purification. Methanol (liquid chromatography−mass spectrometry (LC−MS) grade), water (LC−MS grade), and formic acid (LC−MS grade) were purchased from Fisher-Scientific (Leicestershire, U.K.). Stocks (1 mg/mL) of Pep-01 to Pep-08 (see Table 1) in methanol/water/formic acid (39.9:60:0.1) were diluted in methanol/water/formic acid (49.5:49.5:1) to a final concentration of ∼1.0 μM. Tryptic peptides were obtained from Thermo Scientific (Waltham, MA) and diluted to 100 μL in water.

Electron Capture Dissociation Mass Spectrometry. Samples were introduced to a 7 Tesla solariX-XR (Bruker Daltonics, Bremen, Germany) mass spectrometer equipped with a ParaCell via static positive ion mode nanospray ionization (nESI) with pulled glass capillaries (P-97 Flaming/Brown micropipette puller tip Sutter Instrument Company, Novato, CA). The capillary voltage was 800 V, and the temperature was 120 °C. Peptide ions were isolated in the quadrupole (isolation width 5 m/z) prior to fragmentation by ECD. ECD was performed by the use of thermal electrons at a current of 1.50 A, with a cathode bias of 0.6 V and a lens potential of 10 V. The pulse length was varied between 0.1 and 0.5 s according to each precursor ion. Data analysis was performed with Data Analysis 4.2 software (Bruker Daltonics) and manually searched for a, x, $c^{\bullet}/c$, b, y, $z/z^{\bullet}$ fragment ions.

Traveling Wave Ion Mobility Mass Spectrometry. TWIMS experiments were performed on a Synapt G2S mass

DOI: 10.1021/acs.jpcb.9b08506
J. Phys. Chem. B 2020, 124, 461−469

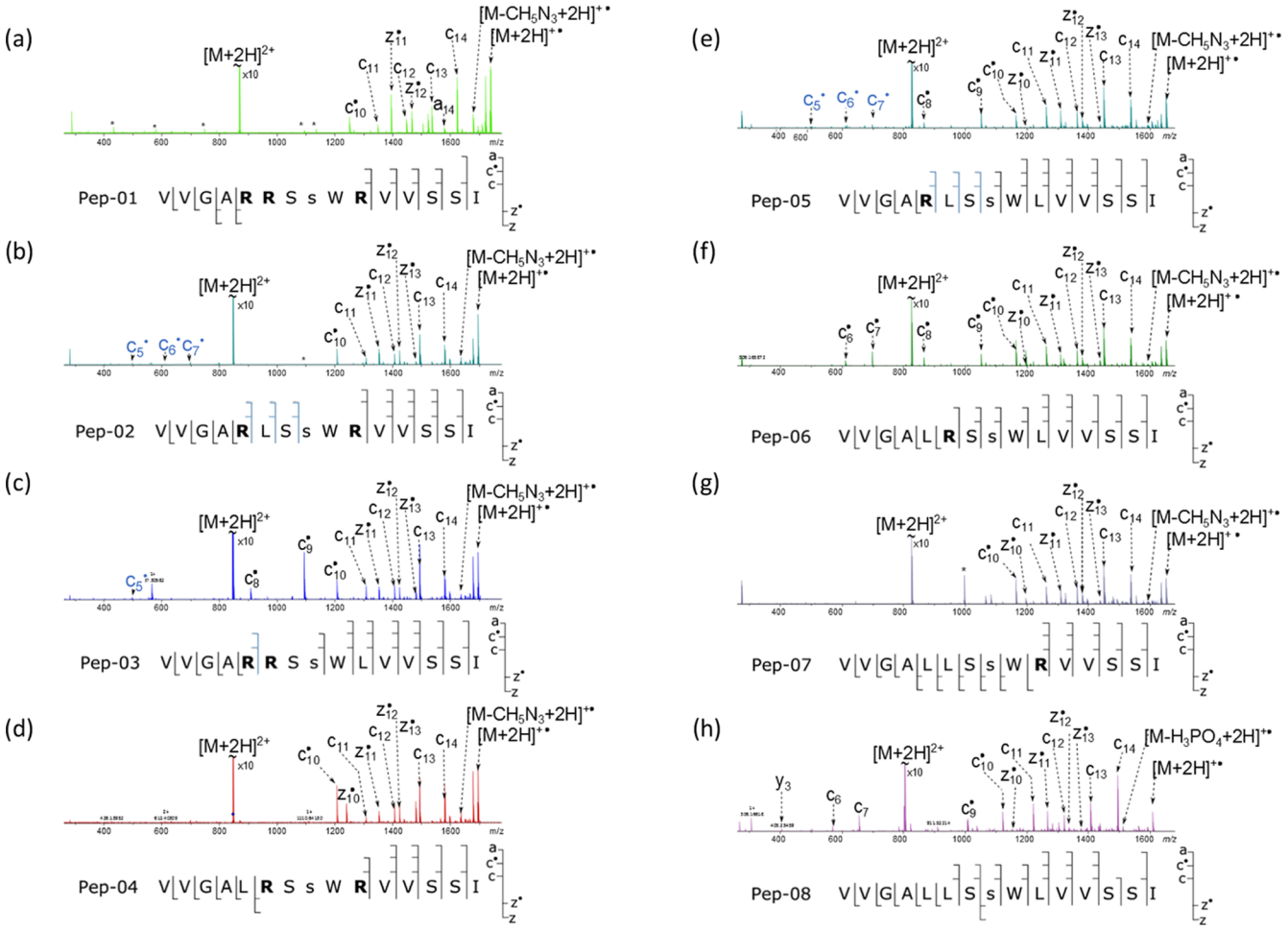

Figure 1. ECD mass spectra and corresponding fragmentation patterns observed for (a) Pep-01, (b) Pep-02, (c) Pep-03, (d) Pep-04, (e) Pep-05, (f) Pep-06, (g) Pep-07, and (h) Pep-08. Low abundance fragments are indicated with blue ticks in the fragmentation pattern and blue labels in the mass spectra.

spectrometer (Waters Corp., Milford, MA) equipped with a Triversa Nanomate nanoelectrospray (nESI) source (Advion, Ithaca, NY). Samples were introduced using nESI voltages in the range of 1.2−1.8 kV and gas pressures of 0.3−0.35 psi. TWIMS was operated at a wave velocity of 450 ms^{-1} and wave amplitudes of 19, 20, and 21 V, with the TWIMS cell maintained at ∼2 mbar of nitrogen. Further information on instrument parameters can be found in Supporting Table S1, while details of the pressure readings observed during these experiments are in Supporting Table S2. Arrival time distributions were produced using a mass range that contained all of the isotopologues of each peptide, and collision cross sections (CCSs) were calculated from the apex value. CCS calibration was performed by an adaptation of the procedure described by Ruotolo et al.[32] Reduced drift time (DT′) of the calibrant ions was calculated by 1

$$DT' = DT - \frac{c\sqrt{m/z}}{1000} \quad (1)$$

where DT is the drift time and c is the "enhanced duty cycle" (EDC) delay coefficient (c = 1.43 for our instrument). Reduced cross section (Ω′) of the calibrant ions was calculated by 2

$$\Omega' = \frac{^{DT}CCS_{He}}{z\sqrt{\frac{1}{\mu}}} \quad (2)$$

where z is the charge of the ion and μ is the reduced mass. A power regression of $\Omega' = A{\cdot}DT'^{b}$ gives values for A and b, which can be used to calculate Ω for the analyte ions by 3

$$CCS_{analyte} = \frac{A{\cdot}z{\cdot}^{TW}DT'_{N_2}{}^{b}}{\sqrt{\mu}} \quad (3)$$

This process was carried out over three wave amplitudes, from which a mean and standard deviation of $CCS_{analyte}$ was calculated. Standards used for calibration were $[M + 2H]^{2+}$ tryptic peptides of BSA, cytochrome c, and myoglobin, with reference drift-tube helium CCS obtained from the Clemmer database.[39] The list of calibrant ions used can be found in Supporting Table S3, and the calibration curves are in Supporting Figure S1. TWIMS data and data processing are reported according to the guidelines published by Gabelica et al.[40] Data acquisition and processing were carried out using MassLynx 4.1 and Driftscope 2.1 software (Waters Corporation, Manchester, U.K.).

Molecular Modeling. Parameters for neutral phosphoserine, neutral arginine, neutral C-terminal isoleucine, and neutral N-terminal valine residues were built in Avogadro 1.2.[41] with

DOI: 10.1021/acs.jpcb.9b08506
J. Phys. Chem. B 2020, 124, 461−469

an acetyl-glycine cap on the N-terminus and an amidated glycine cap at the C-terminus and then optimized using Gaussian 09 (HF 6-31G (d,p)).[42] The electrostatic potential surface of the residue was calculated using the Merz−Singh−Kollman scheme,[43] and the residue was added to a .off library, using the prepgen, parmchk2, and tleap AMBER utility programs. The .off libraries and corresponding .frcmod files for these residues are available online (http://www.biosciences-labs.bham.ac.uk/cooper/datasets.php). Molecular modeling was performed in the AMBER16 suite[44] using the ff99sb and phos10aa forcefields. While these forcefields were developed for solvated proteins and are not as accurate for gas-phase simulations, they are considered suitable for semi-quantitative, gas-phase molecular modeling studies.[45] Simulations were performed using a three-tiered simulated annealing (SA) approach (t_{SA} = 25.2 fs, T = 1000 K; tier 1, n = 1000; tier 2, n = 12 000; tier 3, n = 12 000) from an extended starting structure to produce a 25 000-strong ensemble. MM ensembles were processed using cpptraj.[46] The simulated helium CCS for each of these structures was calculated in IMoS[47] using the trajectory method. A new CCS-matched ensemble was created from models whose simulated CCS was within the experimental CCS ± 5%. Onward analysis of CCS-matched ensembles was performed using MATLAB R2018b (Mathworks, Natick, MA).

Pairwise distances between all atoms were calculated for each model of the CCS-matched ensemble to create an $n_{atoms}^2 \times n_{structures}$ matrix, which was subjected to dimensionality reduction by random projection following the procedure described by Palmer et al.[48] The compression factor of the random projection was optimized on a subset of the ensemble to select the greatest compression factor, from which the ensemble could still be accurately reconstructed. For this optimization, the L1 norm of the difference between the original data (M) and the reconstructed data ($Q \times P$) was used as an error metric and calculated for a number of compression factors. Fitting a double exponential to these data and graphically solving for the compression factor at 2/3 the point of maximum curvature gives the optimum compression factor. The projections produced were clustered by k-means (n = 10, Euclidean), and the sum of least-squares method was used to define the structures closest to the centroids of each of the 10 clusters, which would serve as a representative of each cluster.

RESULTS AND DISCUSSION

The sequences, calculated monoisotopic masses, calculated mass-to-charge ratios, and experimentally derived CCS of the doubly protonated ions of the eight phosphopeptides derived from 14-3-3-ζ (Pep-01−Pep-08) are shown in Table 1. Pep-01 corresponds to the wild-type sequence, Pep-02−Pep-04 contains single Arg→Leu substitutions, and Pep-05 to Pep-07 contains two Arg→Leu substitutions. In Pep-08, all arginine residues have been substituted for Leu residues.

Electron Capture Dissociation. Figure 1a shows the ECD mass spectrum of the doubly charged $[VVGARRSsWRVVSSI + 2H]^{2+}$ (Pep-01) peptide ion. The observed fragment ions are summarized in Supporting Table S4. There is an absence of c/z-type ions within the $\mathbf{R}_5\mathbf{R}SsW\mathbf{R}_{10}$ phosphorylated motif, suggesting the presence of interactions between the phosphoserine and the side chain of Arg5 and Arg10. Figure 1b shows the ECD mass spectrum of the peptide with the motif $\mathbf{R}_5LSsW\mathbf{R}_{10}$ (Pep-02), in which Arg6 was replaced with Leu compared to the wild-type motif. A summary of the observed fragments can be found in Supporting Table S5. No fragment ions resulting from cleavage between the phosphoserine and the Arg at position 10 are observed, suggesting an interaction between these two residues. There are, however, very low abundance (i.e., an order of magnitude smaller than the next most abundant) fragment ions observed, resulting from cleavages between the Arg at position 5 and the phosphoserine ($c_5/c_5^\bullet$, $c_6/c_6^\bullet$, and $c_7/c_7^\bullet$), indicated by blue ticks in the fragmentation pattern in Figure 1b. We hypothesize that these fragments may derive from a minor peptide conformation, which lacks an interaction between Arg5 and pSer, and that a major conformation exists, which does contain this interaction. Fragmentation of the major conformer does not result in the formation of $c_5/c_5^\bullet$, $c_6/c_6^\bullet$, and $c_7/c_7^\bullet$, and these fragments are therefore detected in very low abundance as they originate only from the minor conformation. The ECD mass spectrum of Pep-03 (Figure 1c), in which Arg10 is replaced with Leu, lacks fragments between Arg6 and phosphoserine (see Supporting Table S6). There is a very low abundance fragment ($c_5/c_5^\bullet$) between Arg5 and Arg6 (see the blue tick in the fragmentation pattern in Figure 1c), which may again indicate the presence of major conformation(s) in which Arg5 is interacting with pSer and minor conformation(s) where it is not. Figure 1d shows the ECD mass spectrum of Pep-04, in which Arg5 is replaced with Leu. See Supporting Table S7. No fragments were observed within the R_6SsWR_{10} motif in positions 6−9. It is notable that the substitution of Arg10 by Leu (Pep-03) results in the largest difference in the peptide's ECD behavior compared to that of the wild-type fragmentation spectrum, with two additional high abundance fragments being observed. When Arg5 or Arg6 is substituted, the region of the peptides' sequence in which fragments are not observed is more similar to the wild type, especially with low abundance fragments excluded. This observation implies that there is some redundancy between Arg5 and Arg6 in maintaining the fold of the peptide, i.e., if one is not present, the other is available to interact with pSer. The results obtained for these peptides suggest the presence of interactions between phosphoserine and Arg at position $i \pm 2$, which are sufficiently strong to prevent separation of any ECD fragments, provided that another Arg residue is present.

To test this hypothesis, peptides in which two Arg residues were replaced by two Leu residues in the $\mathbf{R}_5\mathbf{R}SsW\mathbf{R}_{10}$ motif, see Table 1 (Pep-05, Pep-06, and Pep-07), were subjected to ECD. The resulting ECD mass spectra show complete fragment coverage, see Figure 1e−g and Supporting Tables S8−S10, although it is notable that for Pep-05, which has the motif $\mathbf{R}_5LSsWL$, the fragment ions observed between the Arg and pSer residues ($c_5/c_5^\bullet$, $c_6/c_6^\bullet$, and $c_7/c_7^\bullet$) are of very low abundance. As with Pep-02 and Pep-03, these fragments (indicated by blue ticks in the fragmentation pattern in Figure 1e) may indicate that there are conformers of Pep-05 in which a noncovalent interaction is present between Arg5 and pSer. These results agree with the previous work in our laboratory, which showed that the presence of a single basic amino acid residue is insufficient to prevent the observation of full fragment coverage by ECD in phosphopeptides.[20] ECD of doubly charged ions of the peptide in which all Arg residues are replaced with Leu residues (Pep-08) also resulted in complete sequence coverage (Figure 1h and Supporting Table S11).

DOI: 10.1021/acs.jpcb.9b08506
J. Phys. Chem. B 2020, 124, 461−469

Ion Mobility Spectrometry and Molecular Modeling. To further investigate the gas-phase structures of these ions, we employed an ion mobility spectrometry−molecular modeling approach. TWIMS arrival time distributions of the doubly charged ions of Pep-01−Pep-08 are shown in Supporting Figure 2, and their corresponding CCS values are shown in Table 1. The focus of the IMS/MM study was placed on Pep-01−Pep-05 as the ECD behavior of these suggested the presence of intramolecular noncovalent interactions between the phosphoserine and arginine residue(s). It was necessary to model several protonation patterns for each peptide owing to the presence of multiple basic residues (i.e., the N-terminal valine and arginine residues), the acidic phosphoserine, and the necessity of maintaining a net charge of 2+ for all of the peptides. The locations of the charges for each protonation pattern are summarized in Table 2, in which the basic residues and phosphoserine are labeled ^{0},$^{+}$, or $^{-}$ to denote whether they are neutral, positive, or negative, respectively.

Table 2. Protonation Patterns Modeled for Each Peptide

peptide	model	sequence
Pep-01	A	V^0 V G A R^+ R^0 S s^0 W R^+ V V S S I
	B	V^+ V G A R^+ R^0 S s^- W R^+ V V S S I
	C	V^+ V G A R^0 R^+ S s^- W R^+ V V S S I
	D	V^0 V G A R^+ R^+ S s^- W R^+ V V S S I
Pep-02	E	V^0 V G A R^+ L^0 S s^0 W R^+ V V S S I
	F	V^+ V G A R^+ L^0 S s^- W R^+ V V S S I
Pep-03	G	V^0 V G A R^+ R^+ S s^0 W L^0 V V S S I
	H	V^+ V G A R^+ R^+ S s^- W L^0 V V S S I
Pep-04	I	V^0 V G A L^0 R^+ S s^0 W R^+ V V S S I
	J	V^+ V G A L^0 R^+ S s^- W R^+ V V S S I
Pep-05	K	V^0 V G A R^+ L^0 S s^0 W L^0 V V S S I

Each of these 11 protonation patterns was modeled by simulated annealing to produce eleven 25 000-strong molecular ensembles, and simulated CCS were calculated for each of those models. By filtering the SA ensembles by $CCS_{experimental}$ ± 5%, we produced a CCS-matched ensemble for each protonation pattern: these ranged in size from 6477 structures to 21386 structures. Dimensionality reduction was performed on each of the CCS-matched ensembles to reduce the computational cost of the onward analysis and to improve the quality of the subsequent clustering. The projections produced by the dimensionality reduction were clustered by *k*-means (n = 10, Euclidean), a method that should find any clusters in the data or, in the absence of any clusters (i.e., the data existing as a continuum), should segment the data into 10 equally sized portions. By finding the structure closest to the centroid of each cluster, it was possible to analyze the noncovalent interaction patterns across each CCS-matched ensemble (assuming that the structure closest to the centroid of each cluster is representative of the whole cluster). These representative structures were grouped according to the noncovalent interactions between the phosphoserine and other pertinent residues (Val1, Arg5, Arg6, Arg10), with a noncovalent interaction being defined as occurring when a proton on one of these four residues was less than 4 Å distance from the phosphorus atom. Distances are measured between the phosphorus atom (as it is the center of the charge on the phosphate group) and the protons on the N-terminus (Val1) and the Arg side chains. We calculate that a P−H distance of 4 Å would bring the van der Waals radius of the proton within the van der Waals radius of at least one of the phosphate oxygen atoms, while also allowing for variations in bond angles and bond lengths from their equilibrium values. A noncovalent interaction defined on these terms was considered to be a salt bridge when it involved a negatively charged phosphorylated residue and a positively charged residue, while a noncovalent interaction between a neutral phosphorylated residue and a positively charged residue was considered an ionic hydrogen bond, as described by Kim et al.[29] Using this process, it was possible to reduce the complexity of the information in each 25 000-strong molecular modeling ensemble to 10 representative structures, i.e., one structure for each of the 10 clusters. Details of the 10 clusters for each CCS-matched ensemble, including the percentage of the CCS-matched ensemble that each representative structure represents, can be found in Supporting Table S12. The information on the noncovalent interactions with pSer across the representative structures for each of the 11 sequences modeled is summarized in Supporting Table S13, in which the proton−phosphorus distances for each of the 10 representative structures for model A−K are shown. For each representative structure, proton−phosphorus distances <4 Å are highlighted in red, while distances <4.5 Å are outlined with a red box.

As described above, for each peptide, we interpret a lack of fragments in the experimental ECD mass spectrum between any arginine and the phosphoserine as being indicative of the presence of a noncovalent interaction being present between these residues. For Pep-01, models A−D had no representative structures containing noncovalent interactions consistent with those predicted from the ECD fragmentation pattern (i.e., the absence of fragments between Arg5 and Arg10). Structures D2 and D6 from model D, in which all three arginine residues were protonated and pSer was deprotonated (i.e $[Ser\text{-}PO_4H]^-$), had noncovalent interactions between pSer and Arg5, while protons on Arg10 were just outside the range that we have defined as being a noncovalent interactions (at 4.2 and 4.1 Å, respectively). Although these two structures do not themselves have the noncovalent interactions predicted by the ECD data, they represent clusters that contain many structures in which both Arg5 and Arg10 form noncovalent interactions with pSer. Some 13% of the structures in cluster 2 contain noncovalent interactions consistent with the ECD data, while for cluster 6, 11% of the structures have those noncovalent interactions. These representative structures cumulatively represent 18% of the model D CCS-matched ensemble (i.e., cluster 2 and cluster 6) and are shown in Figure 2a. The interactions in these representative structures are characterized as being salt bridges, as the groups interacting are all charged. Model D is the only protonation pattern that produced any representative structures exhibiting noncovalent interactions that were close to being consistent with the ECD data, suggesting that Pep-01 exists predominantly in this protonation state, i.e., all arginine residues protonated and phosphoserine deprotonated, in the gas phase.

For Pep-02, model F produced a single representative structure with the Arg10−pSer noncovalent interaction consistent with the full ECD fragmentation pattern, including the low abundance $c_5/c_5^\bullet$, $c_6/c_6^\bullet$, and $c_7/c_7^\bullet$ fragments (Figure 2b). This representative structure (F4) represented 12% of the F CCS-matched ensemble. The noncovalent interactions in model F are between two ionic residues, the negative phosphoserine and positive arginine residues, and so are characterized as salt bridges. The representative structure F4

DOI: 10.1021/acs.jpcb.9b08506
J. Phys. Chem. B 2020, 124, 461−469

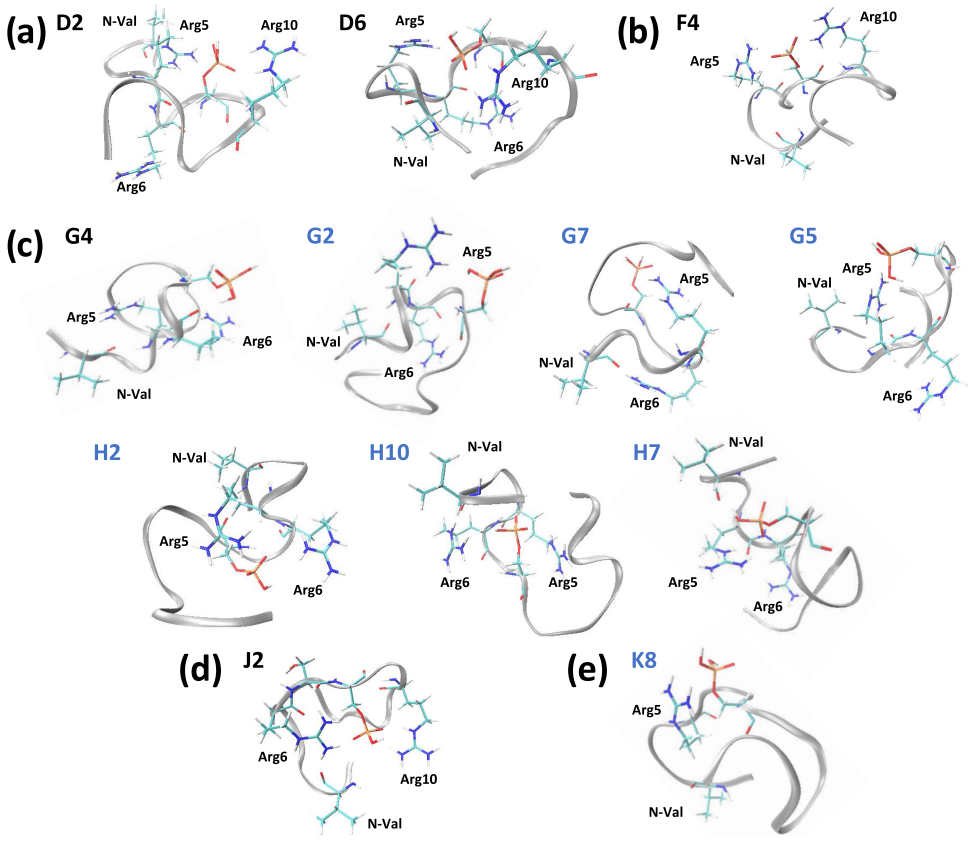

Figure 2. Representative structures with noncovalent interactions consistent with ECD fragmentation patterns for the clustered, CCS-matched modeling ensembles of (a) Pep-01, (b) Pep-02, (c) Pep-03, (d) Pep-04, and (e) Pep-05. Structures are labeled with their model letter and cluster number. Those structures labeled in blue have noncovalent interactions consistent with the ECD data once low abundance fragments have been excluded. Structure J8 only has one of the Arg−pSer interactions predicted by the ECD; the other (Arg6−pSer) is too far (5 Å) to be considered a noncovalent interaction.

does not have both the Arg5−pSer and Arg10−pSer noncovalent interactions that would be consistent with the ECD pattern once low abundance was excluded; however, Arg5 is in close proximity to pSer, with a proton−phosphorus distance of 4.3 Å. It is possible that this represents a weaker Arg5−pSer interaction that hinders the production of fragments in this region but is not sufficiently strong to prevent fragmentation altogether, resulting in the low abundance fragments observed. Alternatively, it is possible that the cluster that F4 represents contains structures with both Arg5 and Arg10 interacting with pSer and that these conformers are responsible for the low abundance of the $c_5/c_5^{\bullet}$, $c_6/c_6^{\bullet}$, and $c_7/c_7^{\bullet}$ fragments.

Model G produced one representative structure whose noncovalent interactions were consistent with the full fragmentation pattern of Pep-03 (Figure 2c). This representative structure (G4) contains an interaction between Arg6 and pSer and could be the conformer from which the c_5 fragment is generated. G4 represents 7% of the model G CCS-matched ensemble. Once the low abundance c_5 fragment is excluded, three further representative structures from model G and three representative structures from model H have the noncovalent interaction Arg5−pSer that is consistent with the ECD data. The three model G representative structures (G2, G7, and G5) all exhibit only the Arg5−pSer interaction and together represent 31% of the model G CCS-matched ensemble. The three representative structures from model H, representing 33% of the H CCS-matched ensemble, also had only the Arg5−pSer interaction, although the representative structure H10 also had protons from the N-terminal valine and Arg6 in close proximity with pSer. We propose G4 as the structure of the minor conformation from which the c_5 fragment arises, while all of the representative structures G2, G7, G5, H2, H10, and H7 are suitable candidates for the structure of the major conformation. As both models G and H produce several representative structures consistent with the proposed fragmentation pattern of the major conformer, we suggest that the two protonation patterns coexist in the gas phase. It should be noted that many of the representative structures produced from models G and H are very similar: G2, G7, and G5 are all structurally similar, as are H2 and H7. A lack of diversity in the representative structures may indicate that the G and H ensembles contain a narrower range of conformers to select from, which is consistent with the observed arrival time distribution for Pep-03, which is narrow relative to the other peptides (Supporting Figure 2).

For Pep-04, no representative structures from either model J or I were consistent with the ECD data, in which no fragments were observed between Arg6 and Arg10, indicating Arg6−pSer and Arg10−pSer noncovalent interactions. For model J, the representative structure of cluster 2 has a salt bridge between Arg6 and pSer and at least one proton on Arg10 within 4.5 Å. While a distance of 4.5 Å is too great to be considered a noncovalent interaction, it is possible that the cluster that this structure represents contains other structures that do have the Arg6−pSer and Arg10−pSer noncovalent interactions that are

DOI: 10.1021/acs.jpcb.9b08506
J. Phys. Chem. B 2020, 124, 461−469

consistent with the ECD data. Examining the whole model J CCS-matched ensemble, 649 of the 14,442 (4%) structures have a proton on both Arg6 and Arg10 within 4 Å of the pSer phosphorus atom, while the protons on the N-terminal valine residue are further than 4 Å from the pSer phosphorus atom, i.e., the salt bridges are consistent with the ECD data. Cluster 2 contains 100 of these ECD-consistent structures; therefore, its representative structure is the most appropriate of those produced and has been selected as the candidate structure for model J (Figure 2d).

For Pep-05 (which contains a single arginine residue), only one sequence (model K) was modeled as there was only one likely combination of charges that produced a net charge of 2+. One representative structure (Figure 2e) was produced that was consistent with the ECD spectrum after the exclusion of low abundance fragments, representing 12% of the ensemble. Eight other representative structures (representing 84% of the K CCS-matched ensemble) had no noncovalent interactions between pertinent residues, which is consistent with the full ECD pattern with low abundance fragments included, in which full fragment coverage was observed and so would not predict the presence of any noncovalent interactions.

CONCLUSIONS

We have shown that the ECD behavior of the doubly charged ions of eight peptides derived from 14-3-3-ζ results in a reduced sequence fragment coverage when there are two or more arginine residues present. These missing regions allowed the locations of noncovalent interactions to be predicted. For the five peptides (Pep-01−Pep-05) for which reduced sequence coverage was observed, we employed an ion mobility spectrometry/molecular modeling workflow to probe the structures of their $[M+2H]^{2+}$ ions further. For Pep-02 where the ECD mass spectrum indicated the presence of conformers with two patterns of noncovalent interactions, the IMS/MM workflow produced a single candidate structure from the model F protonation pattern; this structure had noncovalent interactions consistent with the full ECD fragmentation pattern, though the Arg5 residue was sufficiently near the pSer residue to suggest that it may sometimes interact, leading to the reduced abundance of the $c_5/c_5^{\bullet}$, $c_6/c_6^{\bullet}$, and $c_7/c_7^{\bullet}$ fragments. One representative structure from model G was produced with noncovalent interactions consistent with the ECD data of Pep-03; however, with low abundance fragments excluded, six further representative structures had ECD-consistent noncovalent interactions. These seven representative structures could all serve as candidate structures for Pep-03. No representative structures generated for either Pep-01 or Pep-04 had noncovalent interactions that exactly matched those predicted from the ECD data; however, two structures from model D and one structure from model J had one of the predicted Arg−pSer and the other Arg just outside of interaction distance (<4.5 Å). Closer inspection of the associated clusters showed that they contained many structures that did have noncovalent interactions consistent with the ECD data, making them the most suitable representative structure to propose as candidates. For Pep-05, one structure was proposed as a candidate for the conformation containing the Arg5−pSer noncovalent interaction as indicated by the ECD fragmentation pattern with low abundance fragments removed. With low abundance fragments included, eight possible candidate structures were consistent with the predicted lack of noncovalent interactions between pS8 and positively charged residues.

ASSOCIATED CONTENT

Supporting Information

The Supporting Information is available free of charge at https://pubs.acs.org/doi/10.1021/acs.jpcb.9b08506.

Instrument parameters used and pressure readings observed during TWIMS experiments; list of calibrant ions; fragment ion assignments; information regarding the clusters of CCS-matched ensemble A−K; summary of proton−phosphorus distances; CCS calibration graphs; and arrival time distributions for peptides 1−8 (PDF)

AUTHOR INFORMATION

Corresponding Author

*E-mail: h.j.cooper@bham.ac.uk.

ORCID

David H. Russell: 0000-0003-0830-3914

Helen J. Cooper: 0000-0003-4590-9384

Present Address

[▽]Babraham Institute, Cambridge CB22 3AT, U.K. (A.F.L.-C.).

Author Contributions

[#]A.L.S. and A.F.L.-C. contributed equally to this work.

Notes

The authors declare no competing financial interest.

ACKNOWLEDGMENTS

The authors acknowledge Dr. Lisa Perez of the TAMU Laboratory for Molecular Simulation for insightful discussions and guidance as related to these studies. H.J.C. is an EPSRC Established Career Fellow (EP/L023490/1 and EP/S002979/1). A.F.L.-C. was funded by EPSRC (EP/L023490/1). A.L.S. is funded by the EPSRC Physical Sciences for Health Doctoral Training Centre (EP/L013646/1). D.H.R. is funded by N.I.H. (R01GM121751 and P41GM128577). The Bruker SolariX-XR mass spectrometer was funded by the BBSRC (BB/M012492/1). The Advion Triversa Nanomate and the Waters Synapt G2S mass spectrometer were funded by EPSRC (EP/K039245/1). The authors thank the Centre of Membrane Proteins and Receptors (COMPARE), Universities of Birmingham and Nottingham, Midlands, U.K., for use of their computing facilities. The computations described in this paper were performed using the University of Birmingham's BlueBEAR HPC service, which provides a High Performance Computing service to the University's research community. See http://www.birmingham.ac.uk/bear for more details. Supplementary data supporting this research are openly available from the University of Birmingham data archive at DOI: https://doi.org/10.25500/edata.bham.00000416.

REFERENCES

(1) McLafferty, F. W.; Horn, D. M.; Breuker, K.; Ge, Y.; Lewis, M. A.; Cerda, B.; Zubarev, R. A.; Carpenter, B. K. Electron Capture Dissociation of Gaseous Multiply Charged Ions by Fourier-Transform Ion Cyclotron Resonance. *J. Am. Soc. Mass Spectrom.* **2001**, *12*, 245−9.

(2) Fort, K. L.; Cramer, C. N.; Voinov, V. G.; Vasil'ev, Y. V.; Lopez, N. I.; Beckman, J. S.; Heck, A. J. R. Exploring ECD on a Benchtop Q Exactive Orbitrap Mass Spectrometer. *J. Proteome Res.* **2018**, *17*, 926−933.

DOI: 10.1021/acs.jpcb.9b08506
J. Phys. Chem. B 2020, 124, 461−469

(3) Voinov, V. G.; Deinzer, M. L.; Barofsky, D. F. Electron Capture Dissociation in a Linear Radiofrequency-Free Magnetic Cell. *Rapid Commun. Mass Spectrom.* **2008**, *22*, 3087−8.
(4) Shi, S. D.; Hemling, M. E.; Carr, S. A.; Horn, D. M.; Lindh, I.; McLafferty, F. W. Phosphopeptide/Phosphoprotein Mapping by Electron Capture Dissociation Mass Spectrometry. *Anal. Chem.* **2001**, *73*, 19−22.
(5) Stensballe, A.; Jensen, O. N.; Olsen, J. V.; Haselmann, K. F.; Zubarev, R. A. Electron Capture Dissociation of Singly and Multiply Phosphorylated Peptides. *Rapid Commun. Mass Spectrom.* **2000**, *14*, 1793−800.
(6) Hakansson, K.; Cooper, H. J.; Emmett, M. R.; Costello, C. E.; Marshall, A. G.; Nilsson, C. L. Electron Capture Dissociation and Infrared Multiphoton Dissociation Ms/Ms of an N-Glycosylated Tryptic Peptic to Yield Complementary Sequence Information. *Anal. Chem.* **2001**, *73*, 4530−6.
(7) Kelleher, N. L.; Zubarev, R. A.; Bush, K.; Furie, B.; Furie, B. C.; McLafferty, F. W.; Walsh, C. T. Localization of Labile Posttranslational Modifications by Electron Capture Dissociation: The Case of Gamma-Carboxyglutamic Acid. *Anal. Chem.* **1999**, *71*, 4250−3.
(8) Chalmers, M. J.; Hakansson, K.; Johnson, R.; Smith, R.; Shen, J.; Emmett, M. R.; Marshall, A. G. Protein Kinase a Phosphorylation Characterized by Tandem Fourier Transform Ion Cyclotron Resonance Mass Spectrometry. *Proteomics* **2004**, *4*, 970−81.
(9) Horn, D. M.; Ge, Y.; McLafferty, F. W. Activated Ion Electron Capture Dissociation for Mass Spectral Sequencing of Larger (42 Kda) Proteins. *Anal. Chem.* **2000**, *72*, 4778−84.
(10) Sze, S. K.; Ge, Y.; Oh, H.; McLafferty, F. W. Plasma Electron Capture Dissociation for the Characterization of Large Proteins by Top Down Mass Spectrometry. *Anal. Chem.* **2003**, *75*, 1599−603.
(11) Schnier, P. D.; Price, W. D.; Jockusch, R. A.; Williams, E. R. Blackbody Infrared Radiative Dissociation of Bradykinin and Its Analogues: Energetics, Dynamics, and Evidence for Salt-Bridge Structures in the Gas Phase. *J. Am. Chem. Soc.* **1996**, *118*, 7178−89.
(12) Jackson, S. N.; Dutta, S.; Woods, A. S. The Use of ECD/ETD to Identify the Site of Electrostatic Interaction in Noncovalent Complexes. *J. Am. Soc. Mass Spectrom.* **2009**, *20*, 176−9.
(13) Robinson, C. V.; Chung, E. W.; Kragelund, B. B.; Knudsen, J.; Aplin, R. T.; Poulsen, F. M.; Dobson, C. M. Probing the Nature of Noncovalent Interactions by Mass Spectrometry. A Study of Protein−Coa Ligand Binding and Assembly. *J. Am. Chem. Soc.* **1996**, *118*, 8646−8653.
(14) Kitova, E. N.; Seo, M.; Roy, P. N.; Klassen, J. S. Elucidating the Intermolecular Interactions within a Desolvated Protein-Ligand Complex. An Experimental and Computational Study. *J. Am. Chem. Soc* **2008**, *130*, 1214−26.
(15) Xie, Y.; Zhang, J.; Yin, S.; Loo, J. A. Top-Down Esi-Ecd-Ft-Icr Mass Spectrometry Localizes Noncovalent Protein-Ligand Binding Sites. *J. Am. Chem. Soc.* **2006**, *128*, 14432−3.
(16) Breuker, K.; Oh, H.; Horn, D. M.; Cerda, B. A.; McLafferty, F. W. Detailed Unfolding and Folding of Gaseous Ubiquitin Ions Characterized by Electron Capture Dissociation. *J. Am. Chem. Soc.* **2002**, *124*, 6407−20.
(17) Skinner, O. S.; McLafferty, F. W.; Breuker, K. How Ubiquitin Unfolds after Transfer into the Gas Phase. *J. Am. Soc. Mass Spectrom.* **2012**, *23*, 1011−4.
(18) Breuker, K.; Bruschweiler, S.; Tollinger, M. Electrostatic Stabilization of a Native Protein Structure in the Gas Phase. *Angew. Chem., Int. Ed.* **2011**, *50*, 873−7.
(19) Cui, W.; Zhang, H.; Blankenship, R. E.; Gross, M. L. Electron-Capture Dissociation and Ion Mobility Mass Spectrometry for Characterization of the Hemoglobin Protein Assembly. *Protein Sci* **2015**, *24*, 1325−32.
(20) Harvey, S. R.; Porrini, M.; Tyler, R. C.; MacPhee, C. E.; Volkman, B. F.; Barran, P. E. Electron Capture Dissociation and Drift Tube Ion Mobility-Mass Spectrometry Coupled with Site Directed Mutations Provide Insights into the Conformational Diversity of a Metamorphic Protein. *Phys. Chem. Chem. Phys.* **2015**, *17*, 10538−50.
(21) Lermyte, F.; Sobott, F. Electron Transfer Dissociation Provides Higher-Order Structural Information of Native and Partially Unfolded Protein Complexes. *Proteomics* **2015**, *15*, 2813−22.
(22) Zhang, Z.; Browne, S. J.; Vachet, R. W. Exploring Salt Bridge Structures of Gas-Phase Protein Ions Using Multiple Stages of Electron Transfer and Collision Induced Dissociation. *J. Am. Soc. Mass Spectrom.* **2014**, *25*, 604−13.
(23) Zhang, Z.; Vachet, R. W. Gas-Phase Protein Salt Bridge Stabilities from Collisional Activation and Electron Transfer Dissociation. *Int. J. Mass Spectrom.* **2017**, *420*, 51−56.
(24) Creese, A. J.; Cooper, H. J. The Effect of Phosphorylation on the Electron Capture Dissociation of Peptide Ions. *J. Am. Soc. Mass Spectrom.* **2008**, *19*, 1263−74.
(25) Ruotolo, B. T.; Gillig, K. J.; Woods, A. S.; Egan, T. F.; Ugarov, M. V.; Schultz, J. A.; Russell, D. H. Analysis of Phosphorylated Peptides by Ion Mobility-Mass Spectrometry. *Anal. Chem.* **2004**, *76*, 6727−33.
(26) Ruotolo, B. T.; Verbeck; Thomson, L. M.; Woods, A. S.; Gillig, K. J.; Russell, D. H. Distinguishing between Phosphorylated and Nonphosphorylated Peptides with Ion Mobility−Mass Spectrometry. *J. Proteome Res.* **2002**, *1*, 303−306.
(27) Thalassinos, K.; Grabenauer, M.; Slade, S. E.; Hilton, G. R.; Bowers, M. T.; Scrivens, J. H. Characterization of Phosphorylated Peptides Using Traveling Wave-Based and Drift Cell Ion Mobility Mass Spectrometry. *Anal. Chem.* **2009**, *81*, 248−54.
(28) Lopez-Clavijo, A. F.; Duque-Daza, C. A.; Creese, A. J.; Cooper, H. J. Electron Capture Dissociation Mass Spectrometry of Phosphopeptides: Arginine and Phosphoserine. *Int. J. Mass Spectrom.* **2015**, *390*, 63−70.
(29) Kim, D.; Pai, P. J.; Creese, A. J.; Jones, A. W.; Russell, D. H.; Cooper, H. J. Probing the Electron Capture Dissociation Mass Spectrometry of Phosphopeptides with Traveling Wave Ion Mobility Spectrometry and Molecular Dynamics Simulations. *J. Am. Soc. Mass Spectrom.* **2015**, *26*, 1004−13.
(30) Lanucara, F.; Holman, S. W.; Gray, C. J.; Eyers, C. E. The Power of Ion Mobility-Mass Spectrometry for Structural Characterization and the Study of Conformational Dynamics. *Nat. Chem.* **2014**, *6*, 281−94.
(31) Giles, K.; Pringle, S. D.; Worthington, K. R.; Little, D.; Wildgoose, J. L.; Bateman, R. H. Applications of a Travelling Wave-Based Radio-Frequency-Only Stacked Ring Ion Guide. *Rapid Commun. Mass Spectrom.* **2004**, *18*, 2401−14.
(32) Ruotolo, B. T.; Benesch, J. L.; Sandercock, A. M.; Hyung, S. J.; Robinson, C. V. Ion Mobility-Mass Spectrometry Analysis of Large Protein Complexes. *Nat. Protoc.* **2008**, *3*, 1139−52.
(33) Campuzano, I.; Bush, M. F.; Robinson, C. V.; Beaumont, C.; Richardson, K.; Kim, H.; Kim, H. I. Structural Characterization of Drug-Like Compounds by Ion Mobility Mass Spectrometry: Comparison of Theoretical and Experimentally Derived Nitrogen Collision Cross Sections. *Anal. Chem.* **2012**, *84*, 1026−33.
(34) D'Atri, V.; Porrini, M.; Rosu, F.; Gabelica, V. Linking Molecular Models with Ion Mobility Experiments. Illustration with a Rigid Nucleic Acid Structure. *J. Mass Spectrom.* **2015**, *50*, 711−26.
(35) Moss, C. L.; Chamot-Rooke, J.; Nicol, E.; Brown, J.; Campuzano, I.; Richardson, K.; Williams, J. P.; Bush, M. F.; Bythell, B.; Paizs, B.; et al. Assigning Structures to Gas-Phase Peptide Cations and Cation-Radicals. An Infrared Multiphoton Dissociation, Ion Mobility, Electron Transfer, and Computational Study of a Histidine Peptide Ion. *J. Phys. Chem. B* **2012**, *116*, 3445−56.
(36) Bereszczak, J. Z.; Barbu, I. M.; Tan, M.; Xia, M.; Jiang, X.; van Duijn, E.; Heck, A. J. Structure, Stability and Dynamics of Norovirus P Domain Derived Protein Complexes Studied by Native Mass Spectrometry. *J. Struct. Biol.* **2012**, *177*, 273−82.
(37) Powell, D. W.; Rane, M. J.; Chen, Q.; Singh, S.; McLeish, K. R. Identification of 14-3-3zeta as a Protein Kinase B/Akt Substrate. *J. Biol. Chem.* **2002**, *277*, 21639−42.
(38) Megidish, T.; Cooper, J.; Zhang, L.; Fu, H.; Hakomori, S.; Novel Sphingosine-Dependent, A. Protein Kinase (Sdk1) Specifically

DOI: 10.1021/acs.jpcb.9b08506
J. Phys. Chem. B 2020, 124, 461−469

Phosphorylates Certain Isoforms of 14-3-3 Protein. *J. Biol. Chem.* **1998**, *273*, 21834−45.
(39) Hoaglund, C. S.; Valentine, S. J.; Sporleder, C. R.; Reilly, J. P.; Clemmer, D. E. Three-Dimensional Ion Mobility/Tofms Analysis of Electrosprayed Biomolecules. *Anal Chem* **1998**, *70*, 2236−42.
(40) Gabelica, V.; Shvartsburg, A. A.; Afonso, C.; Barran, P.; Benesch, J. L. P.; Bleiholder, C.; Bowers, M. T.; Bilbao, A.; Bush, M. F.; Campbell, J. L.; et al. Recommendations for Reporting Ion Mobility Mass Spectrometry Measurements. *Mass Spectrom Rev* **2019**, *38*, 291−320.
(41) Hanwell, M. D.; Curtis, D. E.; Lonie, D. C.; Vandermeersch, T.; Zurek, E.; Hutchison, G. R. Avogadro: An Advanced Semantic Chemical Editor, Visualization, and Analysis Platform. *J. Cheminfor.* **2012**, *4*, No. 17.
(42) Frisch, M. J.; Schlegel, H. B.; Scuseria, G. E.; Robb, M. A.; Cheeseman, J. R.; Scalmani, G.; Barone, V.; Petersson, G. A.; Nakatsuji, H.; Li, X.. et al.*Gaussian 09*, revision D.01; Gaussian, Inc.: Wallingford CT, 2016.
(43) Singh, U. C.; Kollman, P. A. An Approach to Computing Electrostatic Charges for Molecules. *J. Comput. Chem.* **1984**, *5*, 129−145.
(44) Case, D. A.; Brozell, S. R.; Cerutti, D. S.; Cheatham, T. E., III; Cruzeiro, V. W. D.; Darden, T. A.; Duke, R. E.; Ghoreishi, D.; Gilson, M. K.; Gohlke, H. et al. *Amber*; University of California: San Francisco, 2016.
(45) Lee, J. H.; Pollert, K.; Konermann, L. Testing the Robustness of Solution Force Fields for Md Simulations on Gaseous Protein Ions. *J. Phys. Chem. B* **2019**, *123*, 6705−6715.
(46) Roe, D. R.; Cheatham, T. E. Ptraj and Cpptraj: Software for Processing and Analysis of Molecular Dynamics Trajectory Data. *J. Chem. Theory Comput.* **2013**, *9*, 3084−3095.
(47) Larriba, C.; Hogan, C. J. Free Molecular Collision Cross Section Calculation Methods for Nanoparticles and Complex Ions with Energy Accommodation. *J. Comput. Phys.* **2013**, *251*, 344−363.
(48) Palmer, A. D.; Bunch, J.; Styles, I. B. The Use of Random Projections for the Analysis of Mass Spectrometry Imaging Data. *J. Am. Soc. Mass Spectrom.* **2015**, *26*, 315−22.

DOI: 10.1021/acs.jpcb.9b08506
J. Phys. Chem. B 2020, 124, 461−469